Previous and current research

Overview

My main area of expertise is UV/Optical the atomic and ionized ISM of star-forming galaxies in the local Universe. For the Lyman Alpha Reference Sample (LARS Hayes et al., 2014; Östlin et al., 2014), I led the analysis of neutral and ionized metal absorption lines HST-COS FUV spectra of the sample galaxies to investigate the relation between kinematic and geometrical properties of the neutral medium, and Lyman α radiative transfer end escape (Rivera-Thorsen et al., 2015, RT15). I re-measured nebular optical emission lines in the SDSS spectra of the sample galaxies, and (re-)computed commonly used diagnostics based on these, which was included in Östlin et al. (2014) and have been adopted as a base line for all later papers about the sample.

I have later revisited the analysis of RT15, now with focus slightly shifted to understand not only Lyα, but also the Lyman Continuum escape of the two first known local-Universe Lyman Continuum leakers, Haro 11 and Tololo 1247-232. The work on the latter is included in Puschnig et al. (submitted), and the work on Haro 11 is on its way in a separate paper (Rivera-Thorsen et al., in prep).

Staying on the topic of local-Universe starbursts, a second major project of mine has been a high-detail, spatially resolved, kinematic multi-component analysis of Optical and NUV nebular emission lines in and around three strongly star-forming knots in local star-forming galaxies ESO 338-IG04 and Haro 11. The analysis has allowed identification of a number of kinematically distinct subsystems, each of which could then be analyzed individually wrt. commonly used line ratio based diagnostics, including dust attenuation, electron density and temperature, ionization, and Oxygen abundance, both the direct T_e-based method and through empirical, strong-line based methods. The results of this work is compiled in Rivera-Thorsen et al. (submitted)

Below, I shall present these main topics in more depth. In addition, I have been involved in smaller projects; I have received training and taken part in the reduction and cleaning of 21 cm. radio interferometric data from the Karl I. Jansky Very Large Array (VLA) of LARS galaxies treated in Pardy et al. (2014); I have reduced VLT/X-Shooter data for Sandberg et al. (2013) and Stritzinger et al. (2014), and performed NUV/Optical observations with the Nordic Optical Telescope on La Palma, Spain, for Sandberg et al. (2015) and other projects.

The Lyman Alpha Reference Sample

The Lyman Alpha Reference Sample (Östlin et al., 2014; Hayes et al., 2014, LARS,) is a sample of 14 + 28 star-forming galaxies at low redshifts, selected for high star formation. I led an analysis of HST-COS spectra of the sample galaxies focusing on the kinematics and geometrical configuration of the neutral ISM. We computed systemic velocities of the sample galaxies from re-measured nebular emission lines in SDSS spectra of the sample galaxies (Östlin et al., 2014, a number of galaxy properties like metallicity etc. derived from these lines were published in the first LARS paper), and measured bulk in-/outflows of the neutral and hot ISM from, mainly, Si II and Si IV absorption lines.

We applied the Apparent Optical Depth method (Savage & Sembach, 1991; Pettini et al., 2002; Quider et al., 2009, e.g.) as implemented by Jones et al. (2013), to disentangle opacity and covering fraction of the neutral gas in metal absorption lines. This method allows a mapping of covering fractions in velocity space, $f_C(v+\delta v)$, by utilizing multiple lines rising from the same ground state of an ion, in this case Si II. In the optically thin limit, the relative depths of these lines are a simple reflection of the lines' oscillator strengths $f\lambda$; but as the column density of the ion grows, the lines grow optically thick, in which case they all have the same depth which reflects the covering fraction of the gas in which they reside. In all cases, both the extremes mentioned above and in intermediate cases, the residual intensity I/I_0 in any given as a function of $f\lambda$, column density N and overing fraction[1] can be fitted to the observed values of I/I_0 and tabular values of $f\lambda$, and best-fit values of N and f_C found for the given bin.

The method is illustrated in Fig. 1 with data for Haro 11 from Rivera-Thorsen et al. (in prep.), where the leftmost panel shows the measured values for three lines, and the red line indicates the bin of interest. Center left panel shows, as black dots, the residual intensities of the lines of the leftmost panels plotted against $f\lambda$,

[1] of gas *with velocities within the bin*.

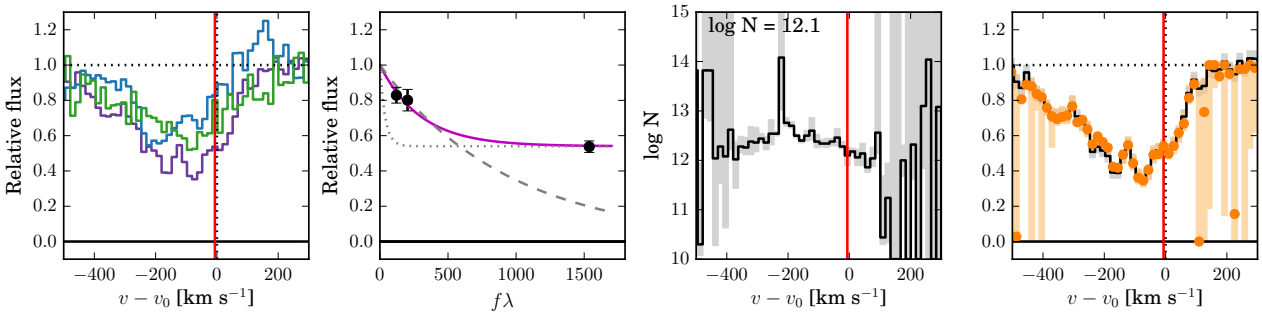

Figure 1: Illustration of the AOD method with example data from Haro 11. **Far left**: Line profile of SiII$\lambda\lambda$1260, 1304, 1526, and a vertical red line denoting the velocity bin of interest for the example. **Center left**: Residual intensity as a function of $f\lambda$ for the three lines. The best fit of $I/I_0(f\lambda)$ is shown in magenta. In gray is shown for illustration I/I_0 in the extreme cases of *a)* unchanged f_C but much higher N (dotted) or *b)* $f_C = 1$ and N 0.5 dex lower. **Center right**: $\log N$ as function of v for these profiles, and **far right**: $1 - f_C$ as function of v (orange circles) superimposed on the profile of Si II 1260 (black steps). Shaded regions are standard errors.

with the best-fit function shown as a magenta curve. In gray is shown the same function with N and f_C varied for illustrative purposes. The center-right panel shows the computed values of $\log N$, and the far-right shows $1 - f_C$ plotted in orange on top of the line profile of Si II, which unlike the other two lines is found to be optically thick everywhere. One should note that since gas at different velocities generally does not occupy the same projected area, f_C only provides a lower limit to the total covering fraction. However, a low f_C max may imply a higher probability of finding direct sight lines through the neutral medium. See RT15 for details.

We finally compared the properties found through spectroscopy, to global properties derived from HST-ACS imaging (Hayes et al., 2014) and VLA 21 cm HI radio interferometry (Pardy et al., 2014). Interestingly, we found a strong anticorrelation between $f_{C,max}$ Hα equivalent width. We tentatively interpreted this as indicating that feedback from strong star formation activity may drive Rayleigh-Taylor instabilities in the outflowing medium, causing it to fragment. An analysis of this kind , but of a larger sample of local galaxies, is a main pillar in both the proposed Hubble Legacy sample and the SAFE sub-projects in this proposal. Combined with insights about the connection between Lyα emission and Lyman Continuum continuum (e.g. Verhamme et al., 2015), this method has also allowed us to constrain the ISM models consistent with Lyman Continuum escape in Tololo 1247-232 (Puschnig et al., submitted) and Haro 11 (Rivera-Thorsen et al, in prep.).

Spatially and kinematically resolved spectroscopy

Another main project of mine has consisted in a spatially-resolved, high-detail analysis of UV/Optical VLT/X-Shooter slit spectra of the recombination nebulae surrounding three starburst regions in nearby galaxies ESO 338-IG04 and Haro 11. The spectra, obtained as part of the X-Shooter Science Verification Program in 2009, were of a high enough S/N ratio that each pixel row could be extracted and measured as an individual spectrum. For each of these, the Hα line was then modeled with 1-5 Gaussian emission line components, constrained such that components must be coherent between neighboring spatial regions. Components which behaved coherently over spatial regions larger than the seeing were then interpreted as originating in the same physical subsystem, assigned an identifying label and grouped this way.

The centroids of the result, for Haro 11 knot B, is shown in the center left panel of Fig. 2, with the y axis being parallel to the slit direction, and the x axis parallel to the dispersion direction. The 2D spectrum is shown under the centroids for comparison. Assuming that Hα was present in all regions that also emitted in other strong lines (which turned out to be a good approximation), we then used the Hα line structure as a template to fit a number of other lines, including Hβ and a number of forbidden metal lines, from which a number of diagnostics could then be computed on a per-component and per-subsystem basis, as well as for the entire collapsed spectrum for better comparison with values reported elsewhere in the literature. This led to a very large and complex amount of computed and measured physical properties in the galaxies, the interpretation of which is too complex and voluminous to cover here. However, I do want to mention one result, partly

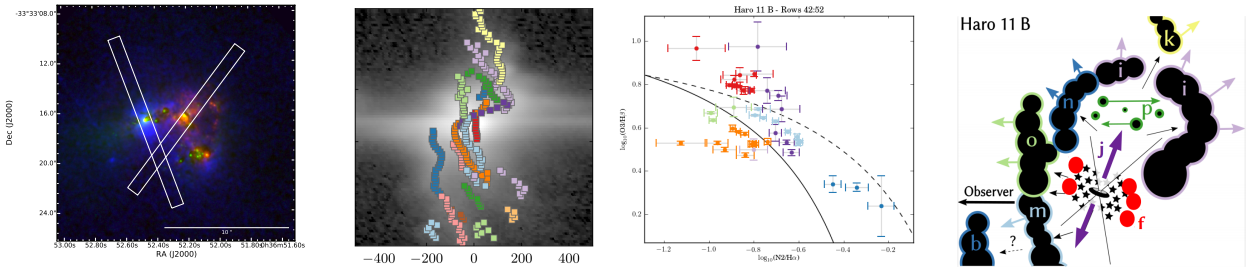

Figure 2: Far left: Slit position on Haro 11. To the right is knot B. **Center left:** Gaussian component centroids overlaid on 2D spectrum of Hα in knot B., colored according to assigned label. **Center left:**BPT diagram of the central area around knot B. **Far right:** Explanatory sketch showing how a configuration of gas, starburst and a central low-luminosity AGN could give rise to a number of the observed components.

because it is exciting, partly because it shows off what the method can do. In a normal BPT analysis, Haro 11 and both its single knots, are placed firmly within the HII/starburst type objects. However, the spatially resolved BPT diagram of the central parts shown in the center-right panel of fig. 2 shows that a couple of components/subsystems stick out, especially the red one (labeled "f" in the paper). This, along with a number of other pieces of circumstantial evidence, all pointed to a low-luminosity, AGN-like object residing deep in the central starburst of knot B[2]. The far-right panel of Fig. 2 sketches how such a constellation of starburst and LLAGN can reproduce a number of the kinematic components observed in this region. It later turned out that this knot has been observed as a hard X-Ray point source with the Chandra X-ray Observatory (Grimes et al., 2007). These observations have been re-evaluated by Prestwich et al. (2015), who concluded, from the x-ray observations alone, that this object was consistent with a high-mass X-Ray Binary seen under very specific circumstances, or with a slowly-accreting intermediate-mass or supermassive black hole. The data have also been evaluated by Basu-Zych et al. (2016) who likewise concluded that it is consistent with a LLAGN-type object. We argue from the kinematics that the HMXB scenario is unlikely, and conclude that it is more likely to be an accreting, massive Black Hole. After the paper went into review, we have further discovered that one component, j in the sketch, is very strong in HeII 4686, with a significant margin too strong to be due to massive stars; a further piece of evidence supporting the LLAGN hypothesis.

References

Basu-Zych, A. R., Lehmer, B., Fragos, T., et al. 2016, , 818, 140

Grimes, J. P., Heckman, T., Strickland, D., et al. 2007, , 668, 891

Hayes, M., Östlin, G., Duval, F., et al. 2014, , 782, 6

Jones, T. A., Ellis, R. S., Schenker, M. A., & Stark, D. P. 2013, , 779, 52

Östlin, G., Hayes, M., Duval, F., et al. 2014,

Pardy, S. A., Cannon, J. M., Östlin, G., et al. 2014, , 794, 101

Pettini, M., Rix, S. A., Steidel, C. C., et al. 2002, , 569, 742

Prestwich, A. H., Jackson, F., Kaaret, P., et al. 2015, , 812, 166

Quider, A. M., Pettini, M., Shapley, A. E., & Steidel, C. C. 2009, , 398, 1263

Rivera-Thorsen, T. E., Hayes, M., Östlin, G., et al. 2015, , 805, 14

Sandberg, A., Guaita, L., Östlin, G., Hayes, M., & Kiaeerad, F. 2015, , 580, A91

Sandberg, A., Östlin, G., Hayes, M., et al. 2013, , 552, A95

Savage, B. D., & Sembach, K. R. 1991, , 379, 245

Stritzinger, M. D., Hsiao, E., Valenti, S., et al. 2014, , 561, A146

Verhamme, A., Orlitová, I., Schaerer, D., & Hayes, M. 2015, , 578, A7

[2] A bit more detail can be found in these slides: http://bit.ly/2e73NLW